Spontaneous Contractility-Mediated Cortical Flow Generates Cell Migration in Three-Dimensional Environments

Rhoda J. Hawkins,[†‡§*] Renaud Poincloux,[‡] Olivier Bénichou,[†] Matthieu Piel,[‡] Philippe Chavrier,[‡] and Raphaël Voituriez[†]

[†]UMR 7600, Université Pierre et Marie Curie/CNRS (Centre National de la Recherche Scientifique), Paris, France; [‡]UMR 144, Institut Curie/CNRS, Paris, France; and [§]Department of Mathematics, University of Bristol, Bristol, United Kingdom

ABSTRACT   We present a model of cell motility generated by actomyosin contraction of the cell cortex. We identify, analytically, dynamical instabilities of the cortex and show that they yield steady-state cortical flows, which, in turn, can induce cell migration in three-dimensional environments. This mechanism relies on the regulation of contractility by myosin, whose transport is explicitly taken into account in the model. Theoretical predictions are compared to experimental data of tumor cells migrating in three-dimensional matrigel and suggest that this mechanism could be a general mode of cell migration in three-dimensional environments.

INTRODUCTION

Beyond its clear interest in the context of cell and molecular biology (1), the study of cell motility and more generally the understanding of simple mechanisms of self-propelled motion is an important challenge for physics and biomimetic technology. Within this context, identifying mechanisms of migration of microorganisms and in particular living cells has motivated numerous works in the biology and physics communities (2,3). Sustained motion at low Reynolds number, the relevant regime at the cell scale, necessitates a constant energy input and therefore requires an active system—i.e., a system driven out of equilibrium by an internal or an external energy source. The cell cytoskeleton has been long identified as an example of such an active system. It is a network of semiflexible filaments made up of protein subunits, interacting with other proteins such as the motor proteins, which make use of the chemical energy of ATP hydrolysis to exert active stresses on the network (1).

Two important out-of-equilibrium processes have been identified as responsible for cell motility: 1), polymerization (treadmilling) of cytoskeleton filaments; and 2), interactions of motor proteins with cytoskeletal filaments, which generally result in the active contraction of the cytoskeleton. In particular, motion induced by actin polymerization (2,3) and spontaneous flows in actomyosin (4) and microtubule-kinesin systems (5) have been observed in vitro, and studied theoretically (6,7) and numerically (8). Based on such cellular mechanisms of force generation, the usual picture of cell locomotion, which relies on classical motility experiments realized on two-dimensional flat substrates, is then as follows: the cell lamellipodium builds strong adhesion points with the substrate and pushes its membrane forward by polymerizing actin. At the back, the actomyosin cytoskeleton contracts the cell body and breaks the adhesion points (1,9).

However, the geometry of the cell environment in vivo is significantly different from a flat substrate. The effect of geometry—and confinement in particular—has been shown to play a crucial role in cell migration, enabling the use of very different mechanisms from that of lamellipodial motility (10,11). In this context, studying cell motility in three-dimensional environments is a promising and widely unexplored field. Recent observations (12) reveal that MDA-MB-231 breast tumor cells migrate in three-dimensional matrigel with a spherical shape (see Fig. 1) according to a contraction-based mechanism in absence of actin protrusion or lamellipodium formation at the leading edge. Here, inspired by these experiments, we develop a model for motility based on the active contraction of the cell's actin cortex that explicitly takes into account the transport of myosin by both cortical flow and free diffusion.

We analytically identify dynamical instabilities of the cortex and demonstrate that steady-state cortical flows, which are observed in many contexts of cell polarization and development (13,14) and usually attributed to preexisting polarization cues, can also appear spontaneously in absence of any preexisting regulatory signals. This suggests a simple mechanism of formation of cortical flows, which is an explicit realization of a mechanism proposed independently in Bois et al. (15) and which we show here can induce cell migration in three-dimensional environments. Theoretical predictions are compared to experimental data of Poincloux et al. (12), and suggest that this contractility-based mechanism could be a general mode of migration in three-dimensional environments that is quite different from the classical picture of lamellipodial motility.
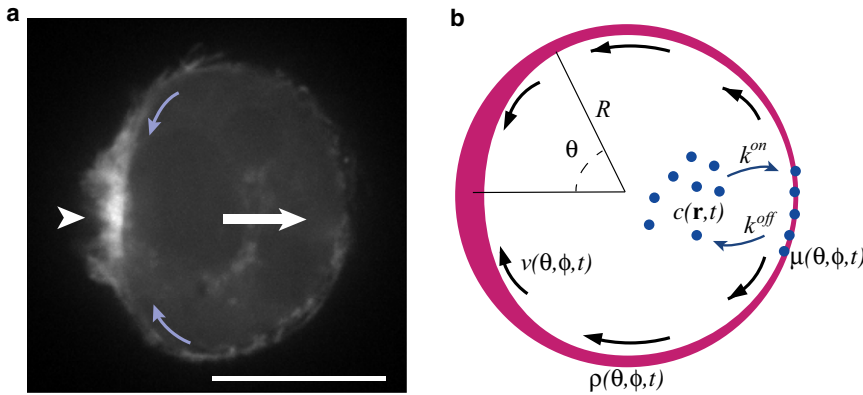
FIGURE 1 Cell migration in three-dimensional environments. (*a*) Confocal section of an MDA-MB-231 cell migrating in three-dimensional matrigel. The cell expresses mCherry-Lifeact, a fluorescent probe that labels F-actin (12). (*White arrow*) Direction of movement. (*Arrowhead*) Accumulation of F-actin at the rear of the cell. (*Curved blue arrows*) Direction of observed cortical flow analyzed in Fig. 3. Scale bar, 10 μm. (*b*) Cartoon of the model in the first unstable mode $Y_{1,0}$, with the actin cortex around the edge (*purple*). (*Arrows*) Velocity of the gel.

MODEL

The model is as follows (see Fig. 1). Motivated by observations of spherically shaped MDA-MB-231 breast tumor cells in three-dimensional matrigel ((12), Fig. 1) we consider a model cell that is geometrically conserved to be spherical (i.e., conserved volume and membrane surface area) with radius R, and use spherical coordinates (r,θ,ϕ). The cell cortex is a thin shell of actomyosin gel that polymerizes at the membrane (which defines the outer boundary at $r = R$) with speed v_p, and depolymerizes with a constant rate k_d. Because the actin cortex can vary in thickness, it can be modeled effectively as a two-dimensional shell of a compressible gel with density $\rho(\theta,\phi,t) = \rho_0(1 + \delta\rho(\theta,\phi,t))$. The average density ρ_0 is set by the polymerization speed v_p according to $\rho_0 = av_p/k_d$, where a is the actin monomer concentration, which for simplicity we assume is constant. Mass conservation is then given by Eq. 1 below. In a first approximation we write the pressure in the cortex $P = \alpha\delta\rho - \beta\nabla^2\delta\rho$, where α^{-1} is the compressibility of the gel and $\sqrt{\beta/\alpha}$ is the correlation length of density fluctuations, and denote $\mathbf{v} = (v_\theta, v_\phi)$ as the components of the gel velocity. Here, we consider only irrotational flows in the cortex and therefore can write $\mathbf{v} = \nabla\psi$. Hereafter the operator ∇ implicitly acts on the angular variables θ,ϕ. We neglect the effects of actin polarization and assume that the gel is in an isotropic phase. The activity of myosin motors then results in a diagonal active stress $-\zeta\mu\delta_{\alpha\beta}$ in the gel, which, following Salbreux et al. (16), we assume is proportional to the local concentration of myosin in the cortex $\mu(\theta,\phi,t)$, where ζ (which here stands for $\zeta\Delta\mu$ in Kruse et al. (6) and Voituriez et al. (7)) is a phenomenological coupling. In the low Reynolds number regime, which is relevant at the cell scale, the force balance in the tangential direction given by Eq. 2 is satisfied, where we denote by ξ the friction with the external medium. Note that our model does not allow deformations from the spherical shape set by the model geometry because this is conserved due to our chosen assumption that the membrane surface area, as well as cell volume, remains constant. We therefore do not write the force balance in the radial direction and our model is limited to conserved spherical geometries, as justified by the shapes observed experimentally (see Fig. 1).

Here we assume for the sake of simplicity that viscous effects in the gel are much smaller than friction (which is here governed by the successive binding and unbinding of transmembrane proteins to the extracellular matrix) and can be neglected as assumed in Callan-Jones et al. (17) in another context. The case of viscosity dominated dynamics, observed in Mayer et al. (14), could be studied along the same lines and yields qualitatively similar results. In the cell bulk, actin filaments are much more diluted than in the cortex and assumed to be in an isotropic phase, so that myosin, whose bulk concentration is denoted by $c(\mathbf{r},t)$, diffuses with diffusion constant D_c (see Eq. 3 where Δ denotes the three-dimensional Laplacian). The myosin motors can attach to the cortex at rate k^{on}, where they are transported with the flow of the actin cortex itself and diffuse with diffusion constant D_μ, and can fall off from the cortex with rate k^{off}. Equation 4

describes the conservation of myosin at the cortex/cytoplasm interface, and Eq. 5 that in the cortex. Drawing all these aspects together, the nonlinear dynamical equations for the system are written as

$$\partial_t\rho + \nabla\cdot(\rho\nabla\psi) = -k_d\rho + av_p = -k_d(\rho - \rho_0), \quad (1)$$

$$\nabla\left(-\zeta\mu - \alpha\delta\rho + \beta\nabla^2\delta\rho\right) = \xi\nabla\psi, \quad (2)$$

$$\partial_t c = D_c\Delta c, \quad (3)$$

$$-D_c\partial_r c|_{r=R} = k^{\mathrm{on}}c(R) - k^{\mathrm{off}}\mu, \quad (4)$$

$$\partial_t\mu + \nabla\cdot(\mu\nabla\psi) = k^{\mathrm{on}}c(R) - k^{\mathrm{off}}\mu + D_\mu\nabla^2\mu. \quad (5)$$

The homogeneous static solution of Eqs. 1–5 is trivially given by $\psi = \delta\rho = 0$, $\mu = \mu_0$, and $c = k^{\mathrm{off}}\mu_0/k^{\mathrm{on}}$. In this case, there is no actin flow in the cortex and the cell is at rest. To determine the linear stability of this homogeneous state, we consider a perturbation of the (l,m) spherical harmonic for each variable. Namely, we let $c(r,\theta,\phi) = c_0 + c_{l,m}(r)\,Y_{l,m}(\theta,\phi)e^{st}$, where c_0 is the homogeneous static solution given by $c_0 = k^{\mathrm{off}}\mu_0/k^{\mathrm{on}}$, and the other (l,m) components of the perturbation are similarly defined as $\psi_{l,m}$, $\delta\rho_{l,m}$, and $\mu_{l,m}$. Solving Eq. 3 then gives $c_{l,m}(r) = \tilde{c}_{l,m}I_{l+1/2}(r\sqrt{s/D_c})/\sqrt{r}$ in terms of the Bessel function I_n. It is then straightforward to obtain a linearized homogeneous system in the variables $\psi_{l,m}$, $\delta\rho_{l,m}$, $\mu_{l,m}$, and $\tilde{c}_{l,m}$,

$$s\delta\rho_{l,m} + k_d\delta\rho_{l,m} - \frac{l(l+1)}{R^2}\psi_{l,m} = 0, \quad (6)$$

$$-\zeta\mu_{l,m} - \alpha\delta\rho_{l,m} - \beta\frac{l(l+1)}{R^2}\delta\rho_{l,m} - \xi\psi_{l,m} = 0, \quad (7)$$

$$D_c\big((l+1-k^{\mathrm{on}}R/D_c)I_{l+1/2}(u) - uI_{l-1/2}(u)\big)\tilde{c}_{l,m} \\ + k^{\mathrm{off}}R^{3/2}\mu_{l,m} = 0, \quad (8)$$

$$\left(s + k^{\mathrm{off}} + \frac{l(l+1)}{R^2}D_\mu\right)\mu_{l,m} - \mu_0\frac{l(l+1)}{R^2}\psi_{l,m} \\ - k^{\mathrm{on}}\tilde{c}_{l,m}I_{l+1/2}(u)/\sqrt{R} = 0, \quad (9)$$

where $u \equiv R\sqrt{s/D_c}$. Demanding a nonzero solution of this system yields an explicit equation for s that defines the dispersion relation of the problem.

This nonpolynomial equation can be studied numerically and fully characterizes the linear dynamics of the full three-dimensional problem. The results are shown in Fig. 2 where we have varied l and the activity ζ, keeping all other parameters constant and the root s shown is always the largest real root.

Simplified equations can be obtained, by reformulating the problem in a one-dimensional geometry. We denote by c_1, μ_1, ρ_1, and ψ_1 the one-dimensional variables, which now depend on $\theta \in [-\pi, \pi]$ only and have, therefore, different dimensions to their three-dimensional counterparts. The dynamics of this corresponding one-dimensional problem is obtained by taking $\nabla = (1/R)\partial_\theta$ in Eqs. 1, 2, and 5, and rewriting Eqs. 3 and 4, which yields

$$\partial_t \delta\rho_1 + \frac{1}{R^2}\partial_\theta((1 + \delta\rho_1)\partial_\theta\psi_1) = -k_{d1}\delta\rho_1, \quad (10)$$

$$\partial_\theta\left(-\zeta\mu_1 - \alpha\delta\rho_1 + \frac{\beta}{R^2}\partial_\theta^2\delta\rho_1\right) = \xi\partial_\theta\psi_1, \quad (11)$$

$$\partial_t c_1 = (D_c/R^2)\partial_\theta^2 c_1 - k_1^{on}c_1 + k_1^{off}\mu_1, \quad (12)$$

$$\partial_t \mu_1 + \frac{1}{R^2}\partial_\theta(\mu_1\partial_\theta\psi_1) = k_1^{on}c_1 - k_1^{off}\mu_1 + \frac{D_\mu}{R^2}\partial_\theta^2\mu_1. \quad (13)$$

Note that the parameter k_1^{on} has a different dimension in one-dimension (units of s^{-1}) than its three-dimensional counterpart (units of $\mu m\ s^{-1}$) but that k_1^{off} and k_{d1} are the same as in three dimensions (units of s^{-1}). The other parameters are kept unchanged. The dispersion relation of this one-dimensional problem is cubic in s and reads for a wave vector k as

$$\begin{aligned}&\left((s + D_c k^2)(s + k_1^{off} + D_\mu k^2) + k_1^{on}(s + D_\mu k^2)\right) \\ &\times (\xi(s + k_{d1}) + k^2(\alpha + \beta k^2)) \\ &+ \zeta\mu_0 k^2(s + k_{d1})(s + k_1^{on} + D_c k^2) = 0.\end{aligned} \quad (14)$$

Actually, this one-dimensional dispersion relation provides a good approximation of the exact dispersion relation by making the substitution $k^2 \equiv l(l + 1)/R^2$ and $k_1^{on} \equiv k^{on}/R$, as checked numerically for a biologically relevant range of parameters (see Fig. 2). The use of this one-dimensional approximation can be justified as follows: First, the dependence on ϕ of the three-dimensional problem can dropped, justified by the fact that the linearized problem (Eqs. 6–9) is independent of m, restricting the problem to axisymmetric solutions. Second, if a decoupling of the radial and angular

dependence of c in the three-dimensional problem is assumed, the dependence on r can be dropped and c depends only on θ as in the one-dimensional problem. Third, and finally, the substitution $k^2 \equiv l(l + 1)/R^2$ identifies the spectrum of the Laplace operator in one dimension with that in three dimensions, allowing the comparison of the two cases.

Making use of the one-dimensional dispersion relation of Eq. 14, we find that beyond the critical value defined by

$$Pe = \frac{-\zeta\mu_0}{\tilde{D}\xi} > Pe_c, \quad (15)$$

where $\tilde{D} = (D_c k_1^{off} + D_\mu k_1^{on})/k_1^{on}$, real positive solutions for s exist for $l \geq 1$, which means that the homogeneous state is unstable and that cortical flows appear. The Péclet number Pe (see also Bois et al. (15)) describes the relative importance of diffusive and advective transport, and is here controlled by both the diffusion properties of myosin, which clearly stabilize the concentration profile, and the amplitude of the advective cortical flow that is governed by the friction and active contractile stress. The critical value Pe_c is obtained numerically from Eq. 14, which reveals that s is maximized for a finite mode l_{max} that grows with Pe (see Fig. 2). The mode l_{max} will therefore be dominant at short times and characterize the developing flow pattern.

To discuss the long time behavior, a nonlinear treatment is necessary. Numerical simulations of the one-dimensional problem (see Eqs. 10–13) show that, above Pe_c, the system reaches a nonhomogeneous steady state (shown in Fig. 3) characterized by a nonvanishing steady-state cortical flow. It should be noted that although the linear analysis at short times is expected to be robust, the long time limit depends on the nonlinearities in the system; here we choose to consider only the convective nonlinearities, keeping in mind that other terms may be relevant.

An analytically tractable model that reproduces this behavior can be derived. In the limit of fast exchange and fast depolymerization (k_1^{on}, k_1^{off}, and k_{d1} larger than D_c/R^2, D_μ/R^2, and $-\zeta\mu_0/(\xi R^2)$), the one-dimensional problem (Eqs. 10–13) can be decoupled and recast to an autonomous equation for μ,

$$R^2\partial_t\mu_1 = \tilde{D}\partial_\theta^2\mu_1 + (\zeta/\xi)\partial_\theta(\mu_1\partial_\theta\mu_1) - \nu\partial_\theta^4\mu_1, \quad (16)$$

which is a type of Keller-Segel equation with drift $-(\zeta/\xi)\partial_\theta\mu_1$ (18) and ν is a phenomenological coupling added to stabilize the system. The transformation $\tilde{t} = \tilde{D}t/R^2$, $\tilde{\nu} = \nu/\tilde{D}$, and $\tilde{\mu} = -\zeta\mu/(\xi\tilde{D})$ makes Eq. 16 dimensionless with the single parameter $\tilde{\nu}$, and one has simply $Pe = \tilde{\mu}_0$ as a control parameter. A linear analysis of this dimensionless equation around the homogeneous solution $\tilde{\mu}_0$ shows that the effective diffusion coefficient, defined as the coefficient of $\partial_\theta^2\tilde{\mu}$, becomes negative for $Pe > 1$. This is
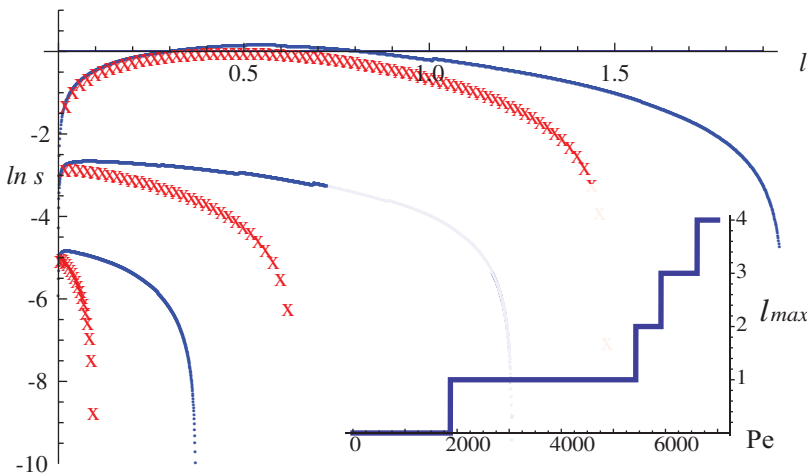

FIGURE 2 Dispersion relation $s(l)$ in log scale. (*Blue lines*) One dimension (where $k = \sqrt{l(l+1)}/R$). (*Red crosses*) Three dimensions. Pairs of curves in ascending order are for $Pe = 500$, 2500, and 5000 (where Pe is defined in Eq. 15). (*Inset*) Most unstable integer mode number l_{max} against Pe. Order-of-magnitude estimates of biologically relevant parameters values taken from the indicated articles are as follows: $k^{on} = 1\ \mu m\ s^{-1}$ (23); $k^{off} = 0.1\ s^{-1}$ (23); $D_c = 10\ \mu m^2\ s^{-1}$ (21,22); $D_\mu = 1\ \mu m^2\ s^{-1}$, $k_d = 0.1\ s^{-1}$ (17,21,22); $\alpha = 1000\ kg\ \mu m^{-1}\ s^{-2}$ (24); $\beta = 1000\ kg\ \mu m\ s^{-2}$, $\xi = 0.1\ kg\ \mu m^{-3}\ s^{-1}$ (17); and $R = 10\ \mu m$ and $\mu_0 = 10^4\ \mu m^{-2}$ (25,26).
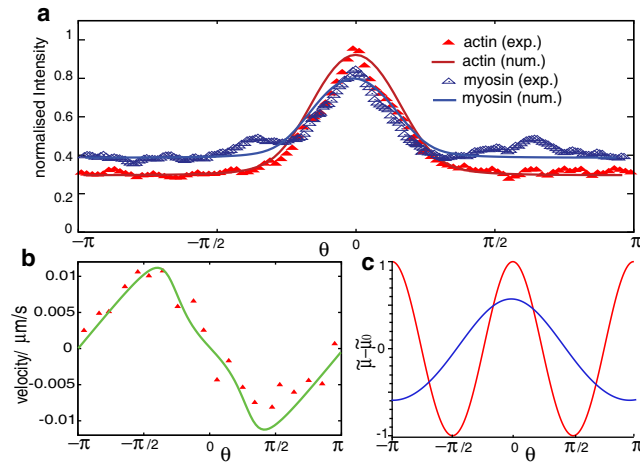
FIGURE 3 (*a*) Experimental data of MDA-MB-231 tumor cells seeded in three-dimensional matrigel (average of 19 cells) (12). Intensity of mCherry-Lifeact labeled cortical actin and labeled myosin are compared to the simulated steady state for ρ and μ with $Pe = 2500$. Maximum and background intensities are fitted. (*b*) (*Red triangles*) Experimental velocity of actin (12) (average of nine cells). (*Green line*) Simulated steady state for *v*. (*c*) Typical patterns for $\tilde{\mu}$ obtained analytically (Eq. 17 with $\tilde{\nu} = 1$): (*blue*) $Pe = 2$; (*red*) $Pe = 5$. Here $\theta \in [-\pi, \pi]$ runs over a given meridian.

commonly referred to as a Lifshitz point, where a transition between a uniform and a modulated phase occurs (19,20). In this context, it is usually necessary to introduce a phenomenological higher-order stabilizing term, which reads $-\nu\partial^4_\theta\mu$ in our example. Here the phenomenological coupling ν is analogous to an effective surface tension and effectively accounts for the stabilizing terms controlled by α and β in the original problem, which were lost in taking the large k_{d1} limit.

A linear stability analysis shows that the homogeneous solution $\tilde{\mu}_0$ is unstable as soon as $Pe > Pe_c = 1 + \tilde{\nu}$, and the most unstable mode is then $l_{\max} = \text{Int}\left(\sqrt{(\tilde{\mu}_0 - 1)/(2\tilde{\nu})}\right)$, where $\text{Int}(x)$ denotes the closest integer to x. The asymptotic nonhomogeneous steady-state solution can then be derived analytically, and reads as

$$\tilde{\mu}(x) = \tilde{\mu}_2 - \left(2\tilde{\mu}_2 + \tilde{\mu}_1 - 3\right)sn^2(y, q), \qquad (17)$$

where sn denotes the Jacobi sine function, $y = (\theta/2)\sqrt{(\tilde{\mu}_2 - \tilde{\mu}_1)/(3\tilde{\nu})}$, and $q = \sqrt{(2\tilde{\mu}_2 + \tilde{\mu}_1 - 3)/(\tilde{\mu}_2 - \tilde{\mu}_1)}$. The constants $\tilde{\mu}_1, \tilde{\mu}_2$ are determined by setting the period to $2\pi/n$ with $n \in \mathbb{N}$ and the mean concentration to $\tilde{\mu}_0$. Typical obtained patterns are shown in Fig. 3 and include multipeaked solutions, which, however, were not seen in the numerical simulations of the full one-dimensional problem (Eqs. 10–13), where solutions seem to relax to single peak profiles, although the full stability analysis of multipeaked solutions has not been done and is left for further work.

RESULTS AND DISCUSSION

These results have implications in the context of cell biology:

First, they show that the regulation of contractility by myosin, which is transported by both cortical flow and free diffusion, is sufficient to destabilize the cortex. This instability leads to steady-state cortical flows, which are observed in many contexts of cell polarization and develop-

ment (13,14), and constitutes an explicit realization of the mechanism proposed independently in Bois et al. (15). Note that this mechanism is closely related to the instability described in Salbreux et al. (16) which, however, relies mainly on calcium dynamics. Although in many examples cortical flows have been shown to rely on preexisting nonhomogeneous regulatory cues, our results show that such cues are not necessary in general, and that systems may exist in which steady-state cortical flows appear spontaneously. The main prediction of the model is that the resulting flow pattern is controlled by *Pe*, as shown in Fig. 2 (where parameter values have been taken from (17,21–26) as indicated in the figure legend). This could be verified experimentally by varying *Pe*, which can be achieved, for instance, by regulating the myosin concentration or activity, or by controlling the friction.

Second, we show that such spontaneous cortical flows can induce motion when the cell is embedded in a three-dimensional medium. The above analysis shows that, for $Pe_c^* > Pe > Pe_c$, the most unstable mode is $l_{\max} = 1$, for which μ, $\delta\rho$, and ψ are proportional to $Y_{1,0}(\theta)$, and creates a converging flow toward the pole $\theta = 0$ of the cell where the cortex thickens, whereas the pole $\theta = \pi$ depletes, as shown in Figs. 1 and 3. Here Pe_c^* denotes the threshold value of *Pe* beyond which $l_{\max} \geq 2$. The friction law of Eq. 2 gives the tangential stress σ_{nt} on the sphere, which can be integrated to yield the propulsion force exerted by the medium on the cell in response to the spontaneous cortical flow. Assuming that the external medium is a very viscous fluid such that the flow in the medium is much slower than the cortical flow in the cell, this propulsion force is nonzero and reads as $F_p = \dfrac{8\pi}{3}h_0R^2\xi v_0$ at linear order, where h_0 is the cortex thickness and v_0 is the amplitude of the cortical flow, showing that the instability of the mode $Y_{1,0}$ induces cell motion. Although the mechanism producing the surface flow is different, this principle is similar to the propulsion of what are known as "squirmers", which are spherical microswimmers with a surface velocity modeled by Blake (27). Note that as the cell moves with constant velocity through the medium, the flow in the external medium must also produce a drag force F_d on the cell (which could be obtained by analyzing the normal stress on the cell surface) so that $F_p + F_d = 0$. Globally, the cell therefore acts on the fluid as a force dipole, as expected for active particles (28).

Third, and finally, we compare these theoretical predictions to experiments conducted on MDA-MB-231 human breast cancer cells seeded in three-dimensional matrigel. These cells were found to migrate in three-dimensional matrigel with a striking round morphology, and to display neither membrane extension nor blebbing at the cell front, in contrast with classical experiments on flat substrates. Silencing the main actin polymerization nucleator found in lamellipodial structures (Arp2/3) had no effect on the cell migration velocity, whereas it is known to be critical

for migration on flat substrates. Moreover, inhibition of myosin II using blebbistatin almost completely abolished cell movement, indicating that myosin activity is essential for movement. We suggest here that the cortical instability studied above, which relies mainly on cortical contractility, could be the mechanism at work under these conditions. High-resolution confocal imaging of live MDA-MB-231 cells in matrigel confirmed a highly nonuniform distribution of cortical actin and myosin, which accumulate at the cell rear (see Fig. 1 and Poincloux et al. (12)). Fig. 3 shows quantitatively the observed actin and myosin profiles, in good agreement with numerical simulations of the model for $Pe > Pe_c$. Analysis of kymographs of these films provided the flow of cortical actin, which is also compatible with the numerical simulations of the model (see Fig. 3). In addition, blocking beta1 integrin function with anti-human beta1 integrin monoclonal antibody 4B4 resulted in a strong reduction in migration and in the presence of blebs. In our model, this corresponds to decreasing the friction parameter ξ and consequently increasing Pe, which leads to a shift of the instability toward the higher modes, which do not yield a nonzero propulsion force on the medium. Together, these experiments (12) suggest that in this example of cell migration in a three-dimensional environment, motility is induced by the cortical instability described in this article. Finally, although direct evidence is lacking at the moment, we suggest that this mechanism could be at work in vivo for different cell types, in particular amoeboid cancer cells (see, for example, A375 melanoma cells in the review by Pinner and Sahai (29)).

CONCLUSION

To conclude, we have presented a generic model of cell motility generated by actomyosin contraction of the cell cortex. We identified analytically dynamical instabilities and showed that spontaneous cortical flow can induce cell migration in three-dimensional environments. Theoretical predictions compare well with experimental data of tumor cells migrating in three-dimensional matrigel, and overall suggest that this contractility-based mechanism of spontaneous cortical flows generation could be a general mode of cell migration in three-dimensional environments, which differs from the classical picture of lamellipodial motility.

REFERENCES

1. Alberts, B. 2002. Molecular Biology of the Cell, 4th Ed. Garland Science, New York.

2. Noireaux, V., R. M. Golsteyn, …, C. Sykes. 2000. Growing an actin gel on spherical surfaces. *Biophys. J.* 78:1643–1654.

3. Bernheim-Groswasser, A., S. Wiesner, …, C. Sykes. 2002. The dynamics of actin-based motility depend on surface parameters. *Nature.* 417:308–311.

4. Smith, D., F. Ziebert, …, J. Käs. 2007. Molecular motor-induced instabilities and cross linkers determine biopolymer organization. *Biophys. J.* 93:4445–4452.

5. Nédélec, F. J., T. Surrey, …, S. Leibler. 1997. Self-organization of microtubules and motors. *Nature.* 389:305–308.

6. Kruse, K., J. F. Joanny, …, K. Sekimoto. 2004. Asters, vortices, and rotating spirals in active gels of polar filaments. *Phys. Rev. Lett.* 92:078101.

7. Voituriez, R., J. F. Joanny, and J. Prost. 2005. Spontaneous flow transition in active polar gels. *Europhys. Lett.* 70:404–410.

8. Marenduzzo, D., E. Orlandini, …, J. M. Yeomans. 2007. Steady-state hydrodynamic instabilities of active liquid crystals: hybrid lattice Boltzmann simulations. *Phys. Rev. E.* 76:031921.

9. Yam, P. T., C. A. Wilson, …, J. A. Theriot. 2007. Actin-myosin network reorganization breaks symmetry at the cell rear to spontaneously initiate polarized cell motility. *J. Cell Biol.* 178:1207–1221.

10. Lämmermann, T., B. L. Bader, …, M. Sixt. 2008. Rapid leukocyte migration by integrin-independent flowing and squeezing. *Nature.* 453:51–55.

11. Hawkins, R. J., M. Piel, …, R. Voituriez. 2009. Pushing off the walls: a mechanism of cell motility in confinement. *Phys. Rev. Lett.* 102:058103.

12. Poincloux, R., O. Collin, …, P. Chavrier. 2011. Contractility of the cell rear drives invasion of breast tumor cells in 3D matrigel. *Proc. Natl. Acad. Sci. USA.* 108:1943–1948.

13. Bray, D., and J. G. White. 1988. Cortical flow in animal cells. *Science.* 239:883–888.

14. Mayer, M., M. Depken, …, S. W. Grill. 2010. Anisotropies in cortical tension reveal the physical basis of polarizing cortical flows. *Nature.* 467:617–621.

15. Bois, J. S., F. Jülicher, and S. W. Grill. 2011. Pattern formation in active fluids. *Phys. Rev. Lett.* 106:028103.

16. Salbreux, G., J. F. Joanny, …, P. Pullarkat. 2007. Shape oscillations of non-adhering fibroblast cells. *Phys. Biol.* 4:268–284.

17. Callan-Jones, A. C., J.-F. Joanny, and J. Prost. 2008. Viscous-fingering-like instability of cell fragments. *Phys. Rev. Lett.* 100:258106.

18. Keller, E. F., and L. A. Segel. 1971. Traveling bands of chemotactic bacteria: a theoretical analysis. *J. Theor. Biol.* 30:235–248.

19. Chaikin, P. M., and T. C. Lubensky. 1995. Principles of Condensed Matter Physics. Cambridge University Press, West Nyack, NY.

20. Yoshinaga, N., J.-F. Joanny, …, P. Marcq. 2010. Polarity patterns of stress fibers. *Phys. Rev. Lett.* 105:238103.

21. Mogilner, A., and L. Edelstein-Keshet. 2002. Regulation of actin dynamics in rapidly moving cells: a quantitative analysis. *Biophys. J.* 83:1237–1258.

22. Pollard, T. D., L. Blanchoin, and R. D. Mullins. 2000. Molecular mechanisms controlling actin filament dynamics in nonmuscle cells. *Annu. Rev. Biophys. Biomol. Struct.* 29:545–576.

23. Hawkins, R. J., O. Bénichou, …, R. Voituriez. 2009. Rebuilding cytoskeleton roads: active-transport-induced polarization of cells. *Phys. Rev. E.* 80:040903.

24. Wagner, O., J. Zinke, …, J. Bereiter-Hahn. 1999. Viscoelastic properties of F-actin, microtubules, F-actin/α-actinin, and F-actin/hexokinase determined in microliter volumes with a novel nondestructive method. *Biophys. J.* 76:2784–2796.

25. Niederman, R., and T. D. Pollard. 1975. Human platelet myosin. II. In vitro assembly and structure of myosin filaments. *J. Cell Biol.* 67:72–92.

26. Kolega, J., and D. L. Taylor. 1993. Gradients in the concentration and assembly of myosin II in living fibroblasts during locomotion and fiber transport. *Mol. Biol. Cell.* 4:819–836.

27. Blake, J. R. 1971. A spherical envelope approach to ciliary propulsion. *J. Fluid Mech.* 46:199–208.

28. Hatwalne, Y., S. Ramaswamy, …, R. A. Simha. 2004. Rheology of active-particle suspensions. *Phys. Rev. Lett.* 92:118101.

29. Pinner, S., and E. Sahai. 2008. Imaging amoeboid cancer cell motility in vivo. *J. Microsc.* 231:441–445.